

Efficient Multimodal Biometric Authentication Using Fast Fingerprint Verification and Enhanced Iris Features

¹A. Jameer Basha, ²V. Palanisamy and ³T. Purusothaman

¹Department of Information Technology,
VLB Janakiammal College of Engineering and Technology Coimbatore, India

²Info Institute of Engineering, Coimbatore, India

³Department of Computer Science and Engineering,
Government College of Technology, Coimbatore, India

Abstract: Problem statement: The accuracy of biometric systems varies with the kind of biometric feature used in it. The Unmoral biometric system is prone to interclass variations. **Approach:** We implement Multimodal biometric systems to overcome the limitations by using multiple pieces of evidence of the same identity. However, the multimodal biometric system is limited to the time constraints due to its multiple processing stages. To improve the speed of authentication in the biometric system with acceptable accuracy, we have introduced a dynamic fingerprint verification technique fused with enhanced iris recognition using the adaptive rank level fusion method. **Results:** When tested upon the standard biometric dataset the system shows improvement in the False Acceptance Rate (FAR) and Equal Error Rate (EER) curves. Essentially, the time taken for the training and verification phase has a reduction of 10% when compared with the existing systems. **Conclusion:** The multimodel system has necessarily increased the speed and performance of the verification system especially when tested on slow processing and low memory devices.

Key words: Multimodal biometrics, fingerprint verification, iris recognition, rank level fusion, iris segmentation, False Acceptance Rate (FAR), Crossing Number (CN, eyelid edge map), Equal Error Rate (EER), biometric system, Genuine Acceptance Ratio (GAR), fingerprint image

INTRODUCTION

Biometrics, which refers to identify an individual based on his or her physiological or behavioral characteristics, can distinguish between an authorized person and an imposter (Ross *et al.*, 2006). Since biometric characteristics are distinctive, cannot be forgotten or lost and the person to be authenticated needs to be physically present at the point of identification, biometrics is inherently more reliable and more capable than traditional knowledge-based and token-based techniques.

In many real-world applications, unimodal biometric systems often face significant limitations due to sensitivity to noise intraclass variability, data quality, non universality and other factors. Attempting to improve the performance of individual matchers in such situations may not prove to be highly effective. Multimodal biometric systems (Veeramachaneni *et al.*, 2005) shown in Fig. 1 seek to alleviate some of these problems by providing

multiple pieces of evidence of the same identity (Kumar *et al.*, 2010; Jain *et al.*, 2004).

These systems help to achieve an increase in performance that may not be possible using a single-biometric indicator.

Fingerprint individuality: Fingerprints are the ridge and furrow patterns on the tip of the finger and have been used extensively for personal identification of people. The biological properties of fingerprint formation are well understood and fingerprints have been used for identification purposes for centuries (Jain *et al.*, 1997a; 1997b)

However, since fingerprint-based biometric systems positive identification with a very high degree of confidence and compact solid state fingerprint sensors can be embedded in various systems (e.g., cellular phones), fingerprint-based authentication is becoming more and more popular in a number of civilian and commercial applications such as, welfare disbursement, cellular phone access and laptop computer log-in.

Corresponding author: A. Jameer Basha, Department of Information Technology,
VLB Janakiammal College of Engineering and Technology Coimbatore, India

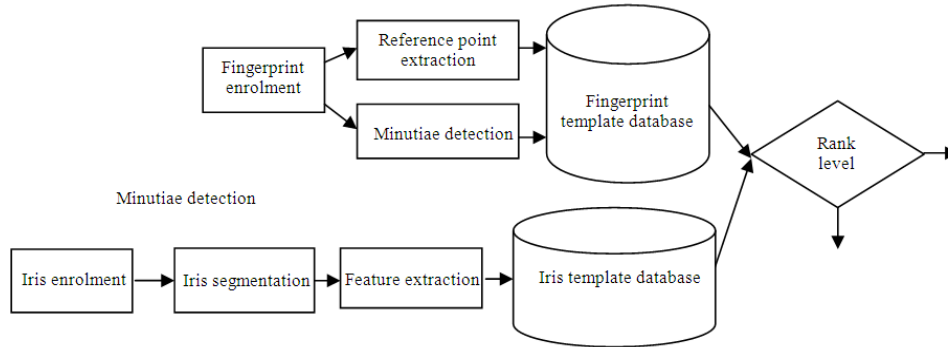


Fig. 1: Logical Structure of the Multimodal System

Iris recognition: The iris is the plainly visible, colored ring that surrounds the pupil. It is a muscular structure that controls the amount of light entering the eye, with intricate details that can be measured, such as striations, pits and furrows (Kong and Zhang, 2001). The iris is not to be confused with the retina, which lines the inside of the back of the eye. There is no detailed correlation between the iris patterns of even identical twins, or the right and left eye of an individual.

MATERIALS AND METHODS

Fingerprint enrolment: The quality of the ridge structures in a fingerprint image is an important characteristic, as the ridges carry the information of characteristic features required for minutiae extraction (Yang *et al.*, 2002). Ideally, in a well-defined fingerprint image, the ridges and valleys should alternate and flow in the locally constant direction. This regularity facilitates the detection of ridges and consequently, allows minutiae to be precisely extracted from the thinned ridges.

Reference point location: Fingerprints have many conspicuous landmarks and any combination of them could be used for establishing a reference point. It is defined the reference point of a fingerprint as the point of maximum curvature of the concave ridges in the fingerprint image (Bazen and Gerez, 2001).

To align two fingerprint images, we must locate a reference point as well as the orientation of each image. The most commonly used reference point is the core point. A core point is defined as the point at which a maximum direction change is detected in the orientation field of a fingerprint image or the point at which the directional field becomes discontinuous.

The most commonly used reference point is the core point. A core point is defined as the point at which a maximum direction change is detected in the orientation

field of a fingerprint image or the point at which the directional field becomes discontinuous. Several methods have been proposed for core point detection.

The reference point or the core point of the fingerprint image is obtained using the following algorithm.

Compute the sine component $\varepsilon(i, j)$ of the smoothed orientation field becomes a reference point:

$$\varepsilon(i, j) = \sin(O'(i, j)) \quad (1)$$

The sine component possesses an attractive characteristic in that it reflects the local ridge direction. A perfectly horizontal ridge has a sine component equals 0. On the other hand, the ridge's sine component equals 1 if it orientates vertically. Due to the discontinuity property, the sine component value always changes abruptly in areas near a reference point. Because of such findings, the following procedure is added.

Initialize a two-dimensional (2-D) array and set all its entries to 0.

Scan the sine component map in a top-to-bottom, left-to-right manner. For each sine component, $\varepsilon(i, j)$

$$\begin{aligned} &O'(i, j) < O' \text{ threshold, } O'(i-1, j) > \frac{\pi}{2}, \text{ - and} \\ &O'(i+1, j) < \frac{\pi}{2}, \text{ then} \end{aligned} \quad (2)$$

- Compute the difference D
- Compute the $C_i(i, j)$ value

For each pixel (i, j) in E, integrate pixel intensities (sine component of the orientation field) in regions RI and RII shown in Fig. 2 and assign the corresponding pixels in A the value of their difference:

$$A(i, j) = \sum_{R_I} \varepsilon(i, j) - \sum_{R_{II}} \varepsilon(i, j) \quad (3)$$

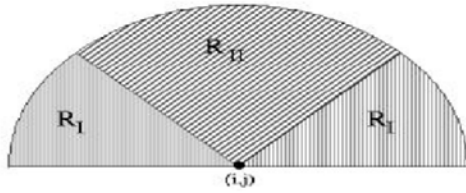


Fig. 2: Regions for integrating pixel intensities in ϵ for computing $A(i, j)$

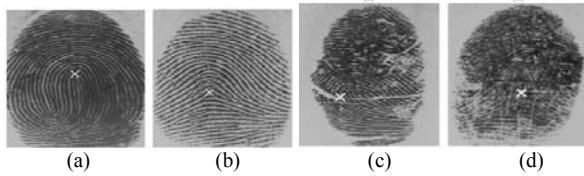


Fig. 3: Examples of the results of our reference point location algorithm



Fig. 4: Example of a ridge ending and a bifurcation

The regions RI and RII (Fig. 2) were determined empirically by applying the reference point location algorithm over a large database. The radius of the semi-circular region was set equal to the window size w . The geometry of regions RI and RII is designed to capture the maximum curvature in concave ridges. Although this approach successfully detects the reference point in most of the cases, including double loops (Fig. 4a), the present implementation is not very precise and consistent for the arch type fingerprints because it is difficult to localize points of high curvature in arch type fingerprint images.

The entry $C_i(i, j)$ is used to compute the continuity of a possible reference point candidate and is defined as shown below:

$$C_i(i, j) = \begin{cases} 1, & C_i(i-1, j-1) + C_i(i-1, j) + C_i(i-1, j+1), \\ \text{if } (i=1) & \\ \text{otherwise} & \end{cases} \quad (4)$$

The difference D in the circular mask indicates the extent of the change of direction for the concave ridges. After all the sine components have been scanned, the position with the maximum value is

obtained. In other words, the location with the sharpest change in the orientation of the ridge direction becomes a reference point.

Due to the presence of noises in a fingerprint image, it is not uncommon that the location with an abrupt change in the orientation field is mistaken as a false reference point. To alleviate the problem, the following conditions must be checked to verify the genuineness of a reference point:

- With the convergence property of the ridges curvature near the reference point, a reference point should be located in the block (i, j) at which the corresponding $C_i(i, j)$ value $> C_{i\text{threshold}}$
- In general, if two reference point candidates have the same D value, the one located at the bottom should be taken as the true reference point

We apply the above procedure using a larger grid size ($w=8$) first and then refine the grid size ($w=3$) to restrict the search in a localized fingerprint image. The method not only increases the processing speed, but also reduces the possible error due to scars or noises in the fingerprint image.

The result of the reference points found in the arch-type fingers is shown in Fig. 3. It can be observed that the locations of the reference points are consistent in different impressions of the same finger.

Minutiae extraction: The endings and bifurcations of the fingerprint images are known as the minutiae (Luo *et al.*, 2000; Maio and Maltoni, 2002) which is shown in the Fig. 4. The most commonly employed method of minutiae extraction is the Crossing Number (CN) concept (Jea and Govindaraju, 2005) This method involves the use of the skeleton image where the ridge flow pattern is eight-connected.

The minutiae are extracted by scanning the local neighborhood of each ridge pixel in the image using a 3×3 window. The CN value is then computed, which is defined as half the sum of the differences between pairs of adjacent pixels in the eight-neighborhood. Using the properties of the CN as shown in Table 1, the ridge pixel can then be classified as a ridge ending, bifurcation or non-minutiae point. For example, a ridge pixel with a CN of one corresponds to a ridge ending and a CN of three corresponds to a bifurcation.

The Crossing Number (CN) method is used to perform minutiae extraction. This method extracts the ridge endings and bifurcations from the skeleton image by examining the local neighborhood of each ridge pixel using a 3×3 window. The CN for a ridge pixel P is given by:

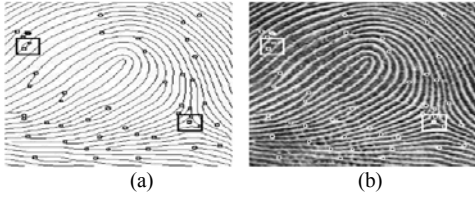


Fig. 5: Results of performing minutiae extraction on a fingerprint image (a) skeleton image (b) original image

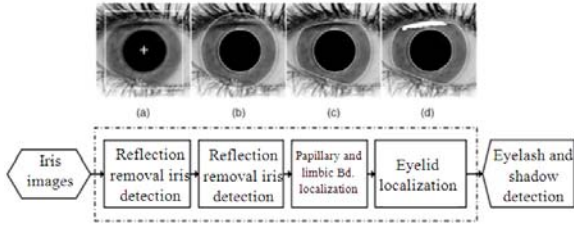


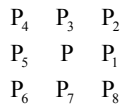
Fig. 6: Flowchart of iris segmentation algorithm

Table 1: The verification performance with different numbers of matching minutiae

Number of matching minutiae	EER (%)	Average radius of the extraction area (pixel)	Ratio of the sub-regions to the full size image
6	8.4%	55	0.185
10	6.4%	79	0.381
18	4.9%	112	0.766

$$CN = 0.5 \sum_{t=1}^8 |P_t - P_{t+1}|, \quad P_9 = P_1 \quad (5)$$

where, P_i is the pixel value in the neighbourhood of P . For a pixel P , its eight neighbouring pixels are scanned in an anti-clockwise direction as follows:



After the CN for a ridge pixel has been computed, the pixel can then be classified according to the property of its CN value. As shown in Fig. 5, a ridge pixel with a CN of one corresponds to a ridge ending and a CN of three corresponds to a bifurcation. For each extracted minutiae point, the following information is recorded:

- x and y coordinates
- orientation of the associated ridge segment
- type of minutiae (ridge ending or bifurcation)

However, there are a few cases where the extracted minutiae do not correspond to true minutiae points in the original image. In addition, it should be noted that in some cases the bifurcation and ridge ending points can be difficult to distinguish between each other. Artifacts of the enhancement stage and thinning process can occasionally result in bifurcations being detected as ridge endings and vice versa.

Hence, in practice, most fingerprint identification systems do not make a distinction between bifurcations and ridge endings when matching minutiae points.

IRIS Recognition: Iris segmentation as shown in the flowchart Fig. 6 is to locate the valid part of the iris for iris biometrics, including finding the pupillary and limbic boundaries of the iris, localizing its upper and lower eyelids if they occlude and detecting and excluding any superimposed occlusions of eyelashes, shadows, or reflections (He *et al.*, 2009).

Being the first step in iris recognition, iris segmentation defines the image contents used for feature extraction and matching, which is directly related to the recognition accuracy. It is reported that most failures to match in iris recognition result from inaccurate iris segmentation. Speed is often a bottleneck in practical applications and iris segmentation is often found to be the most time-consuming module in an iris recognition system. Daugman used the following integrodifferential operator to find the circular boundaries of an iris:

$$\max_{(r, x_0, y_0)} \left| G_{\sigma}(r) * \frac{\partial}{\partial r} \oint_{r, x_0, y_0} \frac{I(x, y)}{2\pi r} ds \right| \quad (6)$$

This operator serves as a circle finder which searches the maximum angular integral of radial derivative over the k -means clustering algorithm on the position and intensity feature vector of the iris image.

Iris detection after reflection removal: The objective of iris detection is not only to identify the presence of an iris in input video sequences but also to determine its position and scale. We use an adaptive threshold T_{ref} to calculate a binary “reflection” map $R_{(x,y)}$ of image $I_{(x,y)}$.

Pupillary and limbic boundary localization: The pupillary and limbic boundaries are modeled as two nonconcentric circles, as usually done in the iris community. Thanks to this particular circular structure, a novel iterative Pulling and Pushing (PP) (Kong and Zhang, 2001; He *et al.*, 2006) as shown in the Fig. 7.

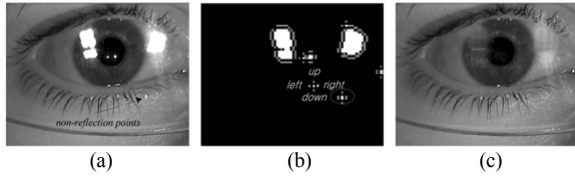


Fig. 7: An original iris image occluded by reflections. (b) The reflection map and the envelop points, denoted with bright and gray points, respectively. (c) The results of reflection removal. Note that, even though several nonreflection points are mistaken as reflection, little harm is made to the iris structure

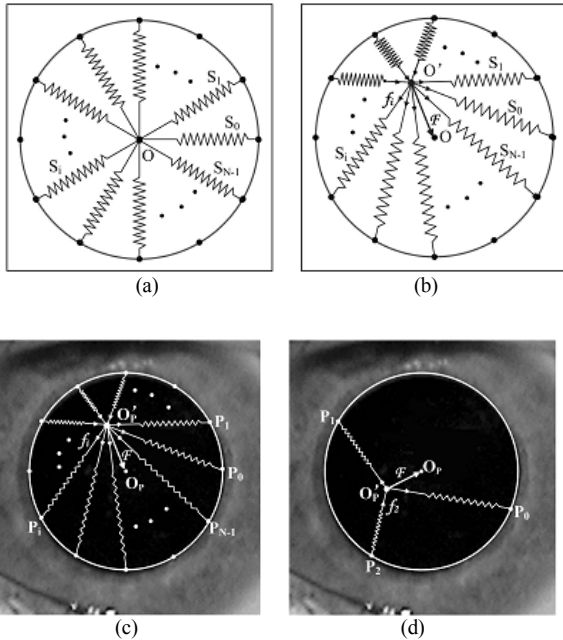


Fig. 8: The basic idea of the PP method. Each “spring” will produce a restoring force to resist its deformation. As a result, the current centre is pulled or pushed until it reaches the equilibrium position. A desirable property is that theoretically only three edge points are required for the PP method to determine the parameters of a circle, as illustrated in (d)

In this section, several important considerations involved in its effective implementation are presented after a brief introduction. Furthermore, we develop a novel EF method based on the PP method for more precise iris localization. This method is useful for dealing with noncircular iris images (e.g., the off-axis ones).

The pulling and pushing method: The inspiration of the PP method stems from Hooke’s law (He *et al.*, 2006) where:

$$\{S_i\}_{i=0}^{N-1} \tag{7}$$

Denotes N identical mass less springs with the equilibrium length R and spring constant k. One end of the springs is attached to circle whose radius is R and the other end joins at point O. At the beginning, all of the springs are relaxed and O is the equilibrium position, as shown in Fig. 8 Then, an appended force is exerted on O to make it move.

To O’ slowly. As a result, ach spring produces a restoring force to resist the introduced deformation:

$$\vec{f}_i = -k(R - r_i)\vec{e}_i, i = 0, 1, \dots, N - 1, \tag{8}$$

Where:

r_i = The current length of s_i

\vec{e}_i = Its direction radiating from O’, $\{\vec{f}_i\}_{i=0}^{N-1}$ will push O’

back to its equilibrium position O after the appended force is removed

Based on such mechanics, the PP method is developed. Let us take the localization of the pupillary boundary as an example (the limbic boundary can be similarly located). Suppose OOP is the rough position of the pupil center obtained by iris detection the PP method then works as follows:

$$\vec{F} = \sum_{i=0}^{N-1} \vec{f}_i \tag{9}$$

Transform the original iris image into polar coordinates (centered by O OP) and perform vertical edge detection on it. Only one edge point along each column is preserved to avoid most of the noisy edge points. In addition, only the $\frac{1}{2}3_{-4}; 9_{-4}$ sector is used to avoid the influence of the upper eyelid occlusion.

Join each resulted edge point:

$$\{P_i\}_{i=0}^{N-1}$$

And the center point O OP with an imaginary spring-like line in the Cartesian coordinates. As a result, we get N identical “springs” attached to a circle and meeting at O OP:

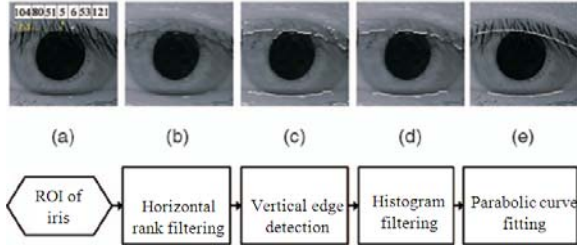


Fig. 9: Flowchart of eyelid localization

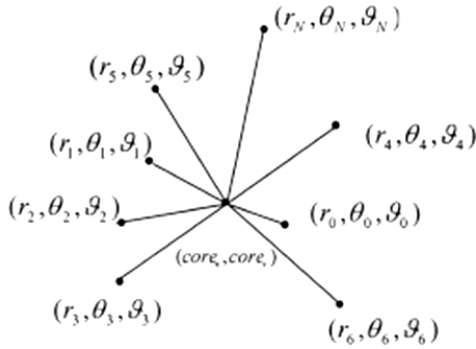


Fig. 10: The first N minutiae and their reference point formed

$$\bar{R} = \frac{1}{N} \cdot \sum_{i=0}^{N-1} O'P_i, k_{pp} = \frac{1}{N} \quad (10)$$

Eyelid localization: The process of the eyelid localization (Kong and Zhang, 2001) is done as shown in the Fig. 9:

- Crop the image ROI, the ROI I_{roi} of the iris image is cropped based on the localization results
- Filter IROI with a 1D horizontal rank filter. With the observation that the eyelashes are mostly vertical thin and dark lines, IROI is horizontally filtered with a 1D rank filter
- Calculate a raw eyelid edge map. Edge detection is then performed on the upper region of I_{ranked} along the vertical direction, resulting in a raw eyelid edge map E_{row} .
- Eliminate noisy edge points via shape similarity Calculation
- Fit the eyelid with a parabola curve. The exact shape of the eyelid is obtained by parabolic curve fitting

Verification and rank-level fusion:

Fingerprint verification: Once the reference point is located, all minutiae extracted from a master fingerprint image can be aligned with the reference point to

generate a circular sub region in the original image (Chan *et al.*, 2004) as shown in Fig. 10. This sub region contains a fixed number of minutiae to be matched with similar minutiae contained in a live template during an authentication process.

First, the Cartesian coordinates of the extracted minutiae in a master fingerprint image are converted into Polar coordinates using the following equations:

$$\begin{aligned} r_i &= \sqrt{(x_i - core_x)^2 + (y_i - core_y)^2} \\ \theta_1 &= \tan^{-1}(y_i - core_y, x_i - core_x) - core_{orient} \\ \vartheta_i &= \phi_i - core_{orient} \end{aligned} \quad (11)$$

Where:

- (x_i, y_i) = Cartesian coordinates of minutia i
- ϕ_i = Minutia orientation
- (r_i, θ) = Polar coordinates of minutia i
- ϑ_i = Normalized minutia orientation
- $(core_x, core_y)$ = Cartesian coordinates of the reference point
- $Core_{orient}$ = Reference point orientation

In polar coordinate representation, the minutiae are rotational and translational invariant with respect to their reference point. After the coordinate's transformation, the minutiae are sorted in ascending order according to their distances from the reference point. To compute a minimum area that covers a predetermined number of minutiae points, we select the first minutiae from the list to form a master feature template (Maio *et al.*, 2002).

Especially in the Arch fingerprints, that some reference points are located near the boundaries of the images. Such cases can lead to large bounding circle size as shown. As a remedy, we construct an average center (X_{center}, Y_{center}) as shown in Fig 11;

$$x_{center} = \sum_{i=0}^N \frac{x_i}{N}, y_{center} = \sum_{i=0}^N \frac{y_i}{N} \quad (12)$$

where, (X_i, Y_i) is the Cartesian coordinates of minutia in the feature template and (X_{center}, Y_{center}) is the new centre of the feature template.

It should be noted that a pre-defined constant R_d is added to tolerate elastic distortion errors during an image capture process. Subsequently, we look for minutiae points only in the bounding circle centered at the average centre.

Adaptive rank level fusion: An effective adaptive rank level fusion scheme that combine information presented by multiple domain experts based on the rank-level fusion integration method (Monwar and GavriloVA, 2009).

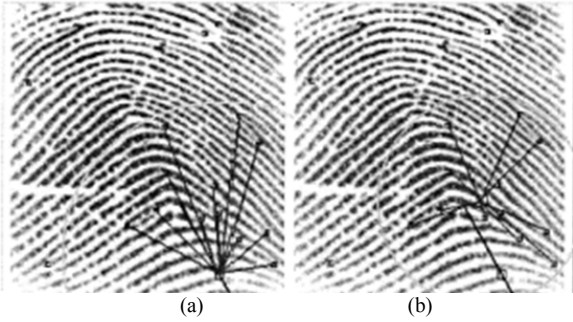


Fig. 11: Size of a bounding circle is large if the reference point is near boundary (b) Size of the bounding circle decreases when a “centralized” reference point is used.

$$R_{\text{Mathing}} = \text{Max}(\sqrt{(x_i - x_{\text{center}})^2 + (y_i - y_{\text{center}})^2}) + R_d$$

$$r_{\text{center}} = \sqrt{(x_{\text{center}} - \text{core}_x)^2 + (y_{\text{center}} - \text{core}_y)^2}$$

$$\theta_{\text{center}} = \tan^{-1} \frac{y_{\text{center}} - \text{core}_y}{x_{\text{center}} - \text{core}_x}$$
(13)

The ranks of individual matchers are combined using the highest rank, approach. The results indicate that fusion of individual modalities can improve the overall performance of the biometric system, even in the presence of low quality data. Insights on multimodal biometric design using rank-level fusion and its performance on a variety of biometric databases are considered.

The main goal is to present a comprehensive analysis of various biometric fusion techniques in combination with advanced biometric feature extraction mechanisms that improve the performance of the biometric information system.

Here we are proposing logistic regression technique in rank level approach. In the logistic regression method, a weighted sum of the individual ranks is calculated.

The weight to be assigned to different matchers is determined by logistic regression. This method is very efficient when different matching modules have significant differences in their accuracies but requires a training phase to determine the weights. It is often not possible to achieve a higher recognition rate and attempting to improve the performance of single matchers in such situations may not prove to be effective due to inherent problems.

By utilizing a multi biometric system, these problems can easily be alleviated by providing multiple pieces of evidence of the same identity, thus achieving higher and more reliable recognition. The proposed system integrates two different biometric matchers of fingerprint and iris and incorporates a rank-level fusion module to improve the recognition performance.

When the output of each biometric matcher is a subset of possible matches sorted in decreasing order of confidence, fusion can be done at the rank level. The goal of rank-level fusion is to consolidate the rank output by individual biometric subsystems (matchers) in order to derive a consensus rank for each identity. In the highest rank method, each possible match is assigned the highest (minimum) rank, as computed by different matchers. The Borda count method uses the sum of the ranks assigned by individual matchers to calculate the final rank. On the other hand, in the logistic regression method, a weighted sum of the individual ranks is calculated.

RESULTS AND DISCUSSION

Fast fingerprint authentication: To evaluate the performance of the fingerprint biometrics system with the reduced number of the minutiae points the 25 fingerprint samples were taken and tested. It is seen from the Table 1 that the EER where the FAR and False Rejection Ratio (FRR) meets at a single point decreases as the number of minutiae points is increased. However, the system is optimized to produce results at a faster rate with a threshold EER score.

Obviously, the processing time of the minutiae extraction process is directly proportional to the image size. If we limit the minutiae extraction to six minutiae, the average bounding circle will have a radius of just 55 pixels. The total minutiae extraction area will be reduced to about 20% of the original size, indicating roughly 20% of the original processing time for the complete image is really needed. The balance between the number of matching minutiae to the FAR and FRR curves is acceptable since the errors rates doesn't significantly changes with the decreasing minutiae count as shown in Fig. 12.

Figure 12 FAR and FRR curves with different number of matching minutiae

Rank level fusion: We compare various biometric techniques in terms of FAR and Genuine Acceptance Ratio (GAR):

$$\text{GAR} = 1 - \text{FRR} \tag{14}$$

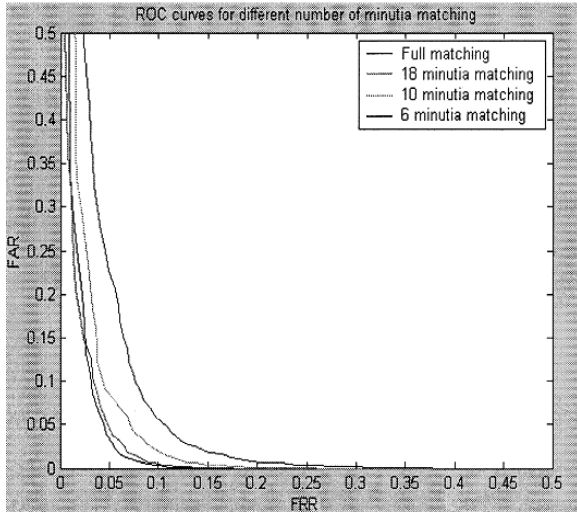


Fig. 12: ROC Curves for different rank level fusion Methods

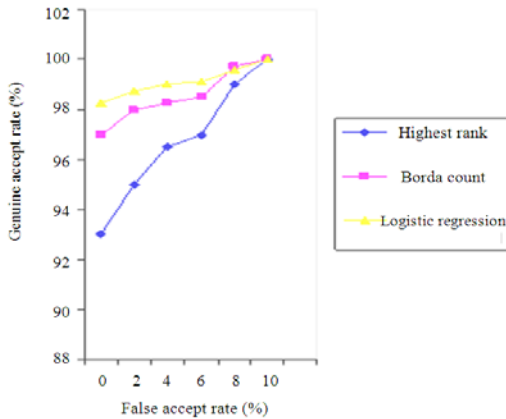


Fig. 13: ROC Curves for different rank level fusion Methods

Table 2: Response time comparison table

Approaches	Training time (min)	Recognition time (min)
Highest Rank method	1.74	0.45
Borda count method	1.74	0.54
Logistic regression method	1.74	0.65

Figure 13 shows the performance rate of three different kinds of rank-level fusion approaches in terms of GAR and FAR. These three different approaches of the rank-level fusion method are as follows: Borda count, Logistic Regression method and Highest Rank method. As noted in the Table 2 the best performance that we have received from this system is using the logistic regression approach of the rank-level fusion method.

In this method, assigning different weights to individual matchers based on their accuracy plays a significant role in determining the final result. The second best result is obtained through the Borda count method. This method is similar to the logistic regression method, except that there is no weight-assigning procedure in this method. This leads to a vital issue on the performance of a biometric system. The least advantage that we obtained through the rank-level fusion method is by using the highest rank method. This method only considers the highest rank associated with each user and can often lead to a problem of lower acceptance rate.

CONCLUSION

The proposed multimodal biometric systems with fingerprint and iris recognition seek to alleviate some of these problems by providing multiple pieces of evidence of the same identity. The time constraints due to its multiple processing stages are overcome by the selecting the sub region of the fingerprint image and iris segmentation techniques given in this study. The adaptive rank level fusion in the multimodal system is fused using rank level fusion at the verification stage. The results show improvements in the fingerprint verification phase and iris segmentation process. The performance of the biometric system shows significant improvement, especially when tested on the slow processing mobile devices. The future scope of our work is to implement the fusion of the multiple biometric evidence during the feature extraction level for improving the accuracy and processing time of the system.

REFERENCES

Bazen, A.M. and S.H. Gerez, 2001. Segmentation of fingerprint images. Laboratory of Signals and Systems. <http://citeseerx.ist.psu.edu/viewdoc/download?doi=10.1.1.122.9683&rep=rep1&type=pdf>

Chan, K.C., Y.S. Moon and Cheng, 2004. Fast fingerprint verification using subregions of fingerprint images. IEEE Trans. Circuits Syst. Video Technol., 14: 95-101. ISSN: 1051-8215

He, Z., T. Tan and Z. Sun, 2006a. Iris localization via pulling and pushing. Proceeding of the 18th International Conference Pattern Recognition, Aug. 20-24, Hong Kong, pp: 366-369. SBN: 0-7695-2521-0

- He, Z., T. Tan, Z. Sun and X. Qiu, 2009. Toward accurate and fast iris segmentation for iris biometrics. *IEEE Trans. Patt. Anal. Mach. Intel.*, 31: 1670-1684. <http://doi.ieeecomputersociety.org/10.1109/TPAMI.2008.183>
- Jain, A.K., A. Ross and S. Pankanti, 2004. An introduction to biometric recognition. *IEEE Trans. Circuits Syst. Video Technol.*, 14: 4-20. ISSN: 1051-8215
- Jain, A.K., H. Lin and R. Bolle, 1997. On-line fingerprint verification. *IEEE Trans. Patt. Anal. Machine Intel.*, 19: 302-314. ISSN: 0162-8828
- Jain, A.K., H. Lin, S. Pankanti and R. Bolle, 1997. An identity-authentication system using fingerprints. *Proc. IEEE*, 85: 1365-1388. ISSN: 0018-9219
- Jea, T.Y. and V. Govindaraju, 2005. A minutia-based partial fingerprint recognition system. *Patt. Recognit.*, 38: 1672-1684. DOI: 10.1016/J.PATCOG.2005.03.016
- Kong, W.K. and D. Zhang, 2001. Accurate iris segmentation based on novel reflection and eyelash detection model. *Proceeding of the International Symposium Intelligent Multimedia, Video and Speech Processing*, May 02-04, Hong Kong, China, pp: 263-266. ISBN: 962-85766-2-3
- Kumar, A., V. Kanhangad and D. Zhang, 2010. A new framework for adaptive multimodal biometrics management. *IEEE Trans. Inform. Forensics Security*, 5: 92-102. SSN: 1556-6013
- Luo, X., J. Tian and Y. Wu, 2000. A minutiae matching algorithm in fingerprint verification. *Proceeding of the 15th International Conference Pattern Recognition*, Sep. 03-07, Barcelona, Spain, pp: 833-836. ISBN: 0-7695-0750-6
- Maio, D. and D. Maltoni, 2002. Direct gray-scale minutiae detection in fingerprints. *IEEE Trans. Patt. Anal. Mach. Intel.*, 19: 27-40. ISSN: 0162-8828
- Maio, D., D. Maltoni, R. Cappelli, J.L. Wayman and A.K. Jain, 2002. VC2000: Fingerprint verification competition. *IEEE Trans. Patt. Anal. Machine Intel.*, 24: 402-412.
- Monwar, M.M. and M.L. Gavrilova, 2009. Multimodal biometric system using rank-level fusion approach. *IEEE Trans. Syst., Man Cybernetics*, 39: 867-878. ISSN: 1083-4419
- Ross, A., K. Nandakumar and A.K. Jain, 2006. *Handbook of Multibiometrics*. 1st Edn., Springer-Verlag, New York, ISBN: 0387222960, pp: 198.
- Veeramachaneni, K., L.A. Osadciw and P.K. Varshney, 2005. An adaptive multimodal biometric management algorithm. *IEEE Trans. Syst. Man Cybern. C Appl. Rev.*, 35: 344-356. ISSN: 1094-6977
- Yang, J., L. Liu and T. Jiang, 2002. An improved method for extraction of fingerprint features. *Proceeding of the 2nd International Conference Image and Graphics (INCIG'02)*, Anhui, China, pp: 1-7. http://nlpr-web.ia.ac.cn/English/mic/jianweiyang/ICIG_yang.pdf